Seismic evidence of extensive microbial gas migration and trapping in submarine gas hydrates (Rakhine Basin, Bay of Bengal)

M. Foschi [a,*], G. Etiope [b], J.A. Cartwright [a]

[a] *Department of Earth Sciences, University of Oxford, South Parks Road, Oxford, OX1 3AN, UK*
[b] *Istituto Nazionale di Geofisica e Vulcanologia, Rome, Italy and Faculty of Environmental Science and Engineering, Babes Bolyai University, Cluj-Napoca, Romania*

ARTICLE INFO

ABSTRACT

Submarine methane-rich gas hydrates in ocean sediments are a potential atmospheric greenhouse gas and energy source. It is considered that microbial methane is generally autochthonous, produced in situ within the gas hydrate stability zone with low gas flux and pressure, while thermogenic gas is allochthonous, migrated from a deeper petroleum system, with higher gas flux and pressure and therefore potentially higher energy resource and environmental impact. Here, we report on the allochthonous nature of large microbial gas hydrate deposits in the Rakhine Basin, Bay of Bengal. An innovative and automatic tool, developed to analyze high-resolution three-dimensional seismic data, allowed to detect hundreds of thousands gas occurrences throughout a 2 km thick Pliocene-Pleistocene sedimentary sequence extending below the gas hydrate stability zone. A supercharged section matching the present-day optimum temperature for microbial methanogenesis was identified. Combining seismic and geochemical data of the Rakhine Basin gas system points to a dominant microbial nature of the gas. Stacked amplitude anomalies and vertical anomaly clusters demonstrate active free-phase gas migration towards the shallow gas hydrate stability zone. The Rakhine Basin gas hydrates are the ultimate seal for the entire petroleum system and represent a case of "frozen seepage" of microbial gas with relatively high flux and pressure.

1. Introduction

Submarine gas hydrates (or clathrates) are a vast reserve of natural gas, primarily methane, amounting to $\sim 3.6 \times 10^6$ Tg CH_4 ($\sim 5 \times 10^{15}$ m^3 CH_4, e.g., Milkov, 2005; Whiticar, 2020), likely larger than the recoverable, proved, methane reserves in sedimentary petroleum systems ($\sim 0.2 \times 10^{15}$ m^3; BP, 2021). The gas hydrates are ice-like crystalline solids composed of rigid cages of water molecules that enclose guest gas molecules, and form in the pores of seafloor sediments where at least 5–10% of gaseous methane is present (Milkov, 2005). One volume of gas hydrates may contain ~ 160 vol of methane at atmospheric temperature and pressure conditions (Kvenvolden, 1995).

Gas hydrates can dissociate, releasing gas, when temperature and pressure decrease below their clathrate stability field (e.g., due to seawater warming; Dillon et al., 2001). Although today the deep-sea hydrates are not a significant source of methane for the atmosphere (e.g., Yamamoto et al., 2009; Etiope, 2015; Ruppel and Kessler, 2017), submarine slumps may trigger local releases of considerable amounts of gas that may reach the atmosphere (Paull et al., 2003). Exploitation of marine hydrates as an energy source requires significant technological challenges to be surmounted, and although global reserves are huge, the gas production may only be economically viable given suitable conditions of local and regional accumulations (e.g., Yamamoto et al., 2019). Both the environmental and energy resources issues are strictly related to the origin and pressure of the gas and its accumulation modality.

Methane in submarine gas hydrates can be autochthonous, produced in situ within a Gas Hydrate Stability Zone (GHSZ), or allochthonous, resulting from "clathratisation" of uplifted conventional reservoirs or gas migration and seepage from deeper reservoirs or source rocks (Beauchamp, 2004; Milkov, 2005; Yang et al., 2021). Autochthonous gas, associated to stratigraphic hydrates (Milkov, 2005), generally refers to microbial methane in low gas flux and accumulation settings (<5% of pores in the GHSZ). Several seismic and modelling studies show examples of submarine hydrates with in-situ methanogenesis (e.g., Malinverno, 2010, Schneider et al., 2014; You et al., 2019). Allochthonous gas, in structural gas hydrates, is typical of higher flux and accumulations of thermogenic gas and subordinately microbial gas (>5%, locally up to 100% of sediment volume; Milkov, 2005). Structural gas hydrates with allochthonous gas clearly represent the preferred target for gas exploitation and for the studies on the potential impact on ocean and

---

* Corresponding author.
  E-mail address: martino.foschi@earth.ox.ac.uk (M. Foschi).

atmosphere methane budget. Distinguishing autochthonous and allochthonous gas in the hydrates is therefore a critical task. The autochthonous vs. allochthonous nature and conditions of the gas can be better assessed by an integrated approach, combining gas geochemical (molecular and isotopic composition) and geophysical (e.g., three-dimensional seismic data) analyses of the entire regional gas-bearing sedimentary system extending below the GHSZ.

Here, we combine high-resolution three-dimensional (3-D) seismic data with published isotopic characterization of the gas from nearby drilled accumulations and derived geothermal gradient from modelling of the base of the GHSZ, to report on the allochthonous nature of large hydrate-gas deposits from the Rakhine Basin, Bay of Bengal, offshore Myanmar (Fig. 1). An innovative automatic tool was developed to detect and catalog seismic amplitude anomalies related to gas occurrences throughout a sedimentary stratigraphic sequence of about 2 km. We analyzed the rationale for these gas occurrences in the context of the wider biogenic (microbial) gas petroleum system known in the region. From this, we develop a model explaining the relationships between the deep gas occurrences, their migration features, and the shallower gas hydrates.

2. Description of the study area

The Rakhine Basin covers an area of 170,000 km^2 and is located to the west of the Myanmar peninsula, in the Bay of Bengal (Fig. 1). The basin is crossed by a dextral strike-slip fault system that separates a coastal folds-thrust system zone to the east (Burma Microplate) and a deep basinal area to the west (India Plate) (Nielsen et al., 2004). The sedimentary column in the study area ranges from 8000 m to nearly 12,000 m to the east (Racey and Ridd, 2015). The sedimentary succession was deposited by the interplay of the westwards sediment supply from the adjacent uplifted Rakhine margin and by the southward distal sediment supply from the paleo-Brahmaputra system (Racey and Ridd, 2015). The sedimentary succession was dominated from the Early to Middle Miocene by NE-SW and NNE-SSW oriented meandering channels and levees which developed during the Late Miocene and the Early Pliocene into more complex channel levees and deep-marine channels, and from the Middle–Late Pliocene into a large distal canyon-system

(Racey and Ridd, 2015). The sedimentary succession was punctured by the deposition of mass transport deposits in late Miocene and late Pliocene as a result of the tectonic instability along the Burma Microplate and the India Plate boundary (Hongxia et al., 2011).

The study area is located entirely in the deep-water basin (license Block AD3), at a water depth of 2050–2500 m (Fig. 1). Pliocene and Pleistocene sediments dominate the stratigraphic column. The boundary between Pliocene and Pleistocene formations is located, on average, at 800 m below the seafloor (Cliff and Carter, 2016). The area is located 150 km south of a zone (license Block A1-A3) where a biogenic (microbial) gas petroleum system was identified (Chung et al., 2012; Cliff and Carter, 2016) and characterized by Middle Miocene to Early Pliocene source rocks (shales) and Late Pliocene reservoirs (turbidite sandstones, 2900–3300 m deep; Chung et al., 2012). The gas, discovered and analyzed from multiple wells about 150 km north of the studied portion of the basin (14 samples at depths of 2900–3300 mbsf) is dominantly microbial (99% vol. CH$_4$, δ^{13}C–CH$_4$: from −59 to −70‰; δ^2H–CH^4: 130 to −250‰; Chung et al., 2012). One-dimensional (1-D) modelling, performed on the same license Block A1-A3 suggested that the organic rich intervals in the shales are thermally immature, but that large quantity of microbial gas has been generated since the Middle Miocene. Most of the gas was supposed to be initially trapped in paleo-hydrates, successively dissociated during progressive sediment burial, with final trapping occurring in Pliocene sandstones sealed by shale interbeds and authigenic carbonate cement beds (Chung et al., 2012). We discuss whether the geophysical data of the gas occurrences in the investigated area are compatible with this northern microbial gas system (license Block A1-A3) in subsequent sections.

3. Materials and Methods

3.1. Materials

We consider a pre-stack time migrated (PSTM) three-dimensional (3-D) seismic volume covering an area of ~12,000 km^2 of the Rakhine Basin (Fig. 1). The 3-D seismic volume, made available for academic research, was processed by the data provider with a standard processing sequence for marine seismic data and finalized to a 0° phase American
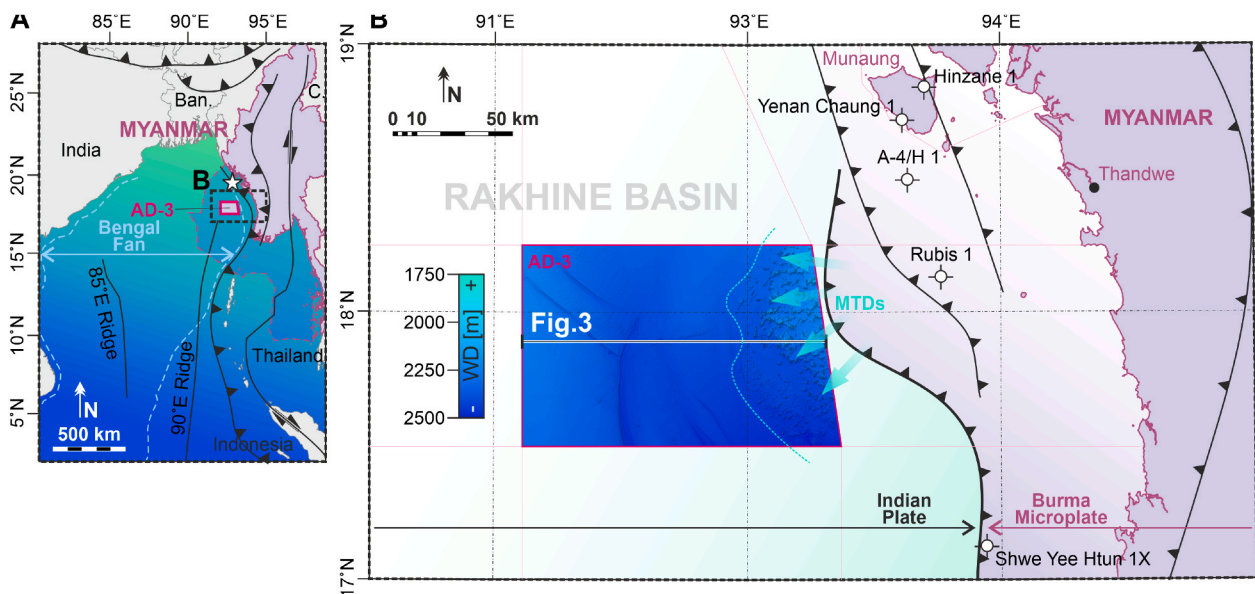

Fig. 1. (A) Location map with position of the exploration license block AD-3, location of the principal microbial gas discoveries (star symbol, license Block A1-A3), main tectonic features, and position of close-up shown in B. The study area is in the eastern portion of the Bengal Fan, also known as the Rakhine Basin, about 150 km from the Myanmar coast. (B) Close up with positions of license block AD-3, coastline, main tectonic features, gas discovery wells, and position of the seismic cross section in Fig. 3. The seafloor depth ranges from 1750 to 2500 m and is characterized to the east by the outcrop of a mass transport deposit originated from the instability along the Burma Microplate and the India Plate boundary. Ban.: Bangladesh; C.: China.

polarity (RC + peak; Brown, 2011). In this work, reflections with a positive excursion of the acoustic impedance with depth, such as the seafloor, will be referred as "hard" reflections, while negative excursions, such as the gas-related amplitude anomalies, as "soft reflections". The sampling interval is 4 ms and the bin spacing is 25 × 37.5 m. The dominant frequency is ~40 Hz and yields a vertical resolution of ~10 m (Widess, 1973). Velocity information was provided as 1-D time-depth table which was used to crudely convert the two-way time (TWT) to depth (from the seismic reference datum, SRD = 0 m to 4 km). Since the seismic data was not depth converted the depth axis (in meters) is not linear (i.e., the depth values have no regular spacing in the presented cross sections). Depths converted from TWT below 4 km were extrapolated. The extrapolated values are included in the cross sections in italic format.

3.2. Methods

The inventory of the gas occurrences along the sedimentary column was carried out using an automatic tool developed in MATLAB (Fig. 2). The gas occurrences are characterized on seismic by very high amplitude response with opposite (reversed) polarity with respect to the seafloor (see later). The tool automatically recognizes these amplitude value on individual time-slices, extracted along the entire trace length of the available database, from 3272 to 4992 ms TWT (430 time slices in total).

The itemized high amplitude samples were used as seed points and for each seed point the system connected adjacent samples characterized by similar amplitude response – the process ended once all the high amplitude samples were linked to form continuous shapes. Because most of the anomalies extend vertically over multiple time-slices, multiple shapes describe the same anomaly. This method increased the absolute
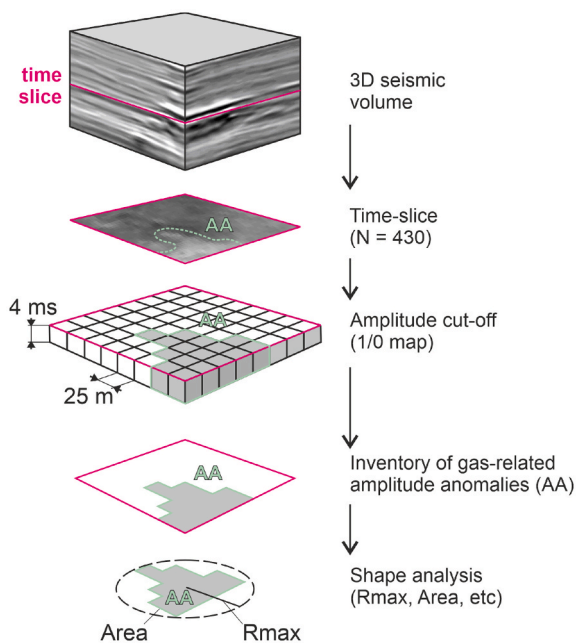

Fig. 2. Workflow for the automatic inventory and analysis of the gas-related amplitude anomalies (AA) encountered in the study area. The initial seismic volume was divided into 430 time-slices, from 3272 (near the seafloor) to 4988 ms TWT, and every 4 ms TWT (same as the sampling interval). For each time slice a logic map (1/0) was created using a fixed amplitude cut off to separate amplified values to background one (see text). Each point on the logic map was used as seed point from where an adaptive 3-by-3 to 5-by-5 window connected adjacent points with similar amplitude values. The generated shapes were then converted into margins and stored into an inventory for each time slice. For each margin geometrical parameters were calculated to generate statistical indicators. The parameters of the margin were manipulated to extract information about the distribution of gas occurrences in the study area (see text).

number of gas related seismic anomalies, but it provided the exact distribution of gas occurrences in the studied interval. The threshold amplitude (dimensionless) that separates high from background amplitude was set to −0.3E4 (see later). The limitation of this method was that acoustically attenuated samples, such as those located at the base of stacked anomalies (c.f., Sheriff, 1975), were not detected and included in the inventory. Nevertheless, the seismic data shows good preservation of the frequency bandwidth with depth implying that the detection is not fully compromised towards the bottom of the survey (see Supplementary Information).

The obtained shapes were converted into margins and used to extract geometrical parameters, such as maximum radius, and area. Three main indicators have been obtained from manipulation of shape parameters. These parameters are (1) AV_{TS}, that is the cumulative amplitude volume of the gas-related amplitude anomalies for each time-slice, expressed as

$$AV_{TS} = \sum_{i=1}^{N} A_i \left(\frac{dt}{2} V_p \right)$$

where N is the number of amplitude margins discovered for each time slice, A_i is the area of the i-th margin, dt is the sampling interval (4E-3 s) and V_p is the compressional velocity, (2) nAA_{TS} that is the number of gas-related amplitude anomaly margins per time-slice (or N, see above), (3) the roundness R, expressed as

$$R = \frac{A}{\pi r_{max}^2}$$

where A is the area of the shape, and r_{max} is the maximum radius of the shape. It is worth noting that AV_{TS} is not indicative of the net volume of gas in place within the anomalies. The latter would require additional parameters of the porous media, such as porosity, and knowledge of the saturation of methane within the calculated amplitude volumes.

The 3-D seismic volume was converted into a root-mean square volume to highlight the presence of gas, and into iso-frequency volumes to enhance the presence of sub-seismic depositional features. The latter analysis was composed of three individual seismic cubes with dominant frequency of 15, 30 and 45 Hz. These frequency volumes were blended using a subtractive model with cyan, magenta, and yellow colors. The 3-D volume attributes were completed using Schlumberger's Petrel software.

The bottom simulating reflection (BSR) present in the study area and interpreted as the base of the gas hydrate stability zone (BGHSZ) (see Results) was used to extrapolate the local geothermal gradient (e.g., Yamano et al., 1982). The stability field for gas hydrate was based on a 100% methane gas composition, a seafloor temperature of 4 °C (Monteleone et al., 2022), and a nominal salinity of 35 PSU. The stability field was modelled using HYDOFF (Sloan and Koh (2007).

4. Results

4.1. Seismic stratigraphic description

The sedimentary infill is imaged on seismic data as a series of parallel eastward-dipping low amplitude reflections associated with the distal deposits of the Ganges-Brahmaputra system (Fig. 3A–C). The individual reflection bound packages, called beds for ease of description in the following sections, are generally isopachous, typically 10–30 m thick. Frequency analysis (see Methods) shows that the predominant seismic facies of the background sedimentary units that are interbedded with channels, levees and MTDs is typical of distal hemipelagic deposits characterized by relatively uniform sheet-like geometry and uniform depositional facies (Fig. 3B) (Brown and Fisher, 1977). Deepwater channels and channel-levees (e.g., Skene et al., 2002) transect this otherwise featureless sedimentary infill (Fig. 3). The channels and channel-levees are distributed across the entire section of the basin but dominate the western and the central portion of the study area (Fig. 3).
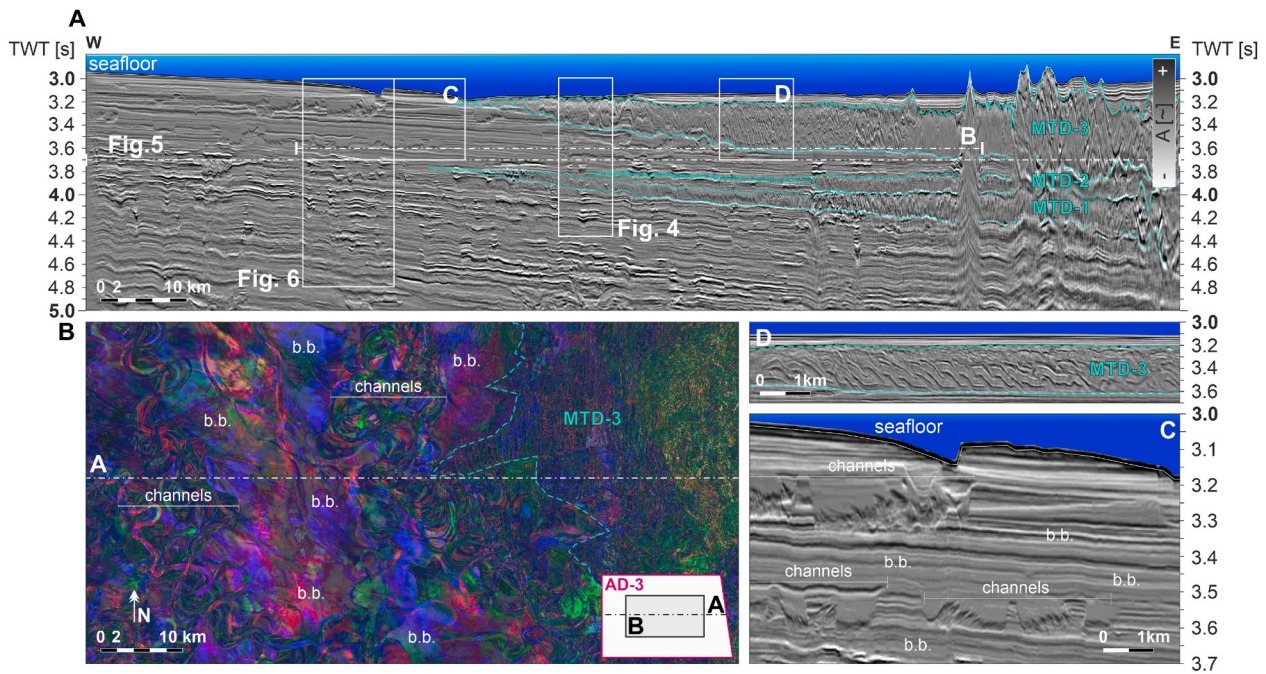
Fig. 3. (A) Representative east-west cross section across the center of the study area (see Fig. 1 for line location) with close-ups and frequency attribute time-slice across the shallow section of the basin (see inset for map location). The sedimentary package is characterized by eastward dipping isopach distal deposits characterized by low amplitude and lateral reflection continuity. The three large MTDs encountered in the study area taper to the west. MTD 3 clearly outcrops at the seafloor where prominent rotated blocks can be observed. (B) The background bedding (b.b.) appears featureless on frequency domain (see Methods) compared with the channels and channel levees and mass transport deposits (MTDs). (C) The background bedding (b.b.) is interrupted by deep-water channels and channels levees characterized by low amplitude response. (D) MTD 3 exhibits an imbricated geometry with a consistent thickness of ~350–400 m (D).

The channels are characterized by a slightly higher acoustic impedance response with respect to the background hemipelagic reflection amplitudes (hard top and soft base; Fig. 3C). The predominantly fine-grained sediments suspected to be filling the channels are however acoustically similar to the hemipelagite background sedimentation. This low contrast in acoustic impedance is responsible for a comparable amplitude response of channels, channel-levees and background bedding on seismic data.

Three large MTDs subdivide the sedimentary infill vertically

(Fig. 3A) in the central and eastern portion of the study area (Fig. 3). MTDs 1 and 2 are located at an average depth of 3750–4000 ms TWT and exhibit a combined average thickness of 200 ms TWT (Fig. 3). MTD 1 and 2 are stacked vertically, but they do not show evidence of cannibalization (Fig. 3A). MTD 3 is in the shallow section of the basin and is part of a more recent large mass transport phenomena originated from the activity of the Burma Microplate and the Indian Plate boundary to the east (Fig. 1B). MTD 3 shows a well-defined imbricated geometry where individual thrust and thrust propagating folds can be observed
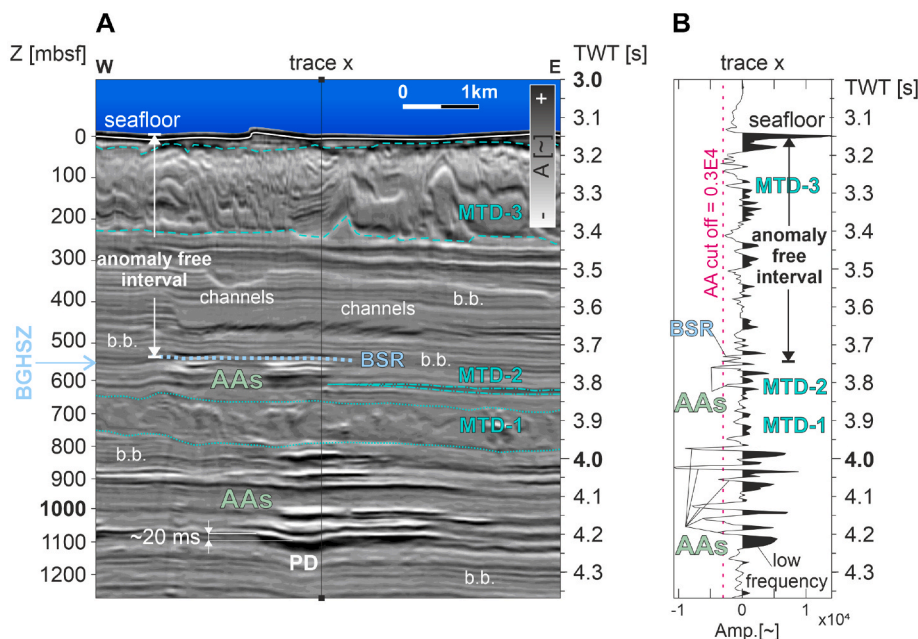

Fig. 4. (A) Seismic cross section depicting a representative example of stacked amplitude anomalies (AAs) encountered within the study area. The microbial gas related AAs are simple soft amplification of the background reflectivity. The AAs are greatly amplified with respect to the background bedding (b.b.), the channels and the mass transport deposits (MTD) and exhibit typically smooth cut-offs between amplified and background regimes. Prominent pushdowns (PD) associated to stacked AAs are observed and are interpreted to be related to gas-induced velocity reductions. A bottom simulating reflection (BSR) is present over much of the study area and it is shown in this cross section at ~560 m. This reflection defines the base of an anomaly-free interval and is interpreted as the base of the gas hydrate stability zone (BGHSZ; see text). (B) Trace x wiggle display shows how prominent are the amplitude anomalies compared to the background reflectivity. The amplitude cut-off, used to separate gas related amplitude anomalies from water bearing sediments, was set to −0.3E4. The amplitude anomalies are also associated with enhanced low frequencies (trace x).

(Fig. 3D). MTD 3 tapers westwards and exhibits an average thickness of 400 ms TWT in its central part. The amplitude of the MTDs is hard at the top and soft at the base, however the amplification of these surfaces is, again, just above the background level.

Overall, the sedimentary infill is acoustically characterized by a relatively modest amplitude excursion with values below the acoustic impedance contrast of ±0.3E4 (Fig. 4, trace x). Even the channels, which are likely to include the coarser members of the grain size distribution

retrieved at Sites U1450 and U1451 (Adhikari et al., 2018) are still weakly amplified (e.g., Fig. 3C). Nevertheless, the acoustic response of the sedimentary infill is largely enhanced by the presence of gas. The reservoirs hosting gas, including the channels, the levees and the MTDs, appear indeed acoustically amplified allowing us to detect the position where free-phase gas is stored within the basin.
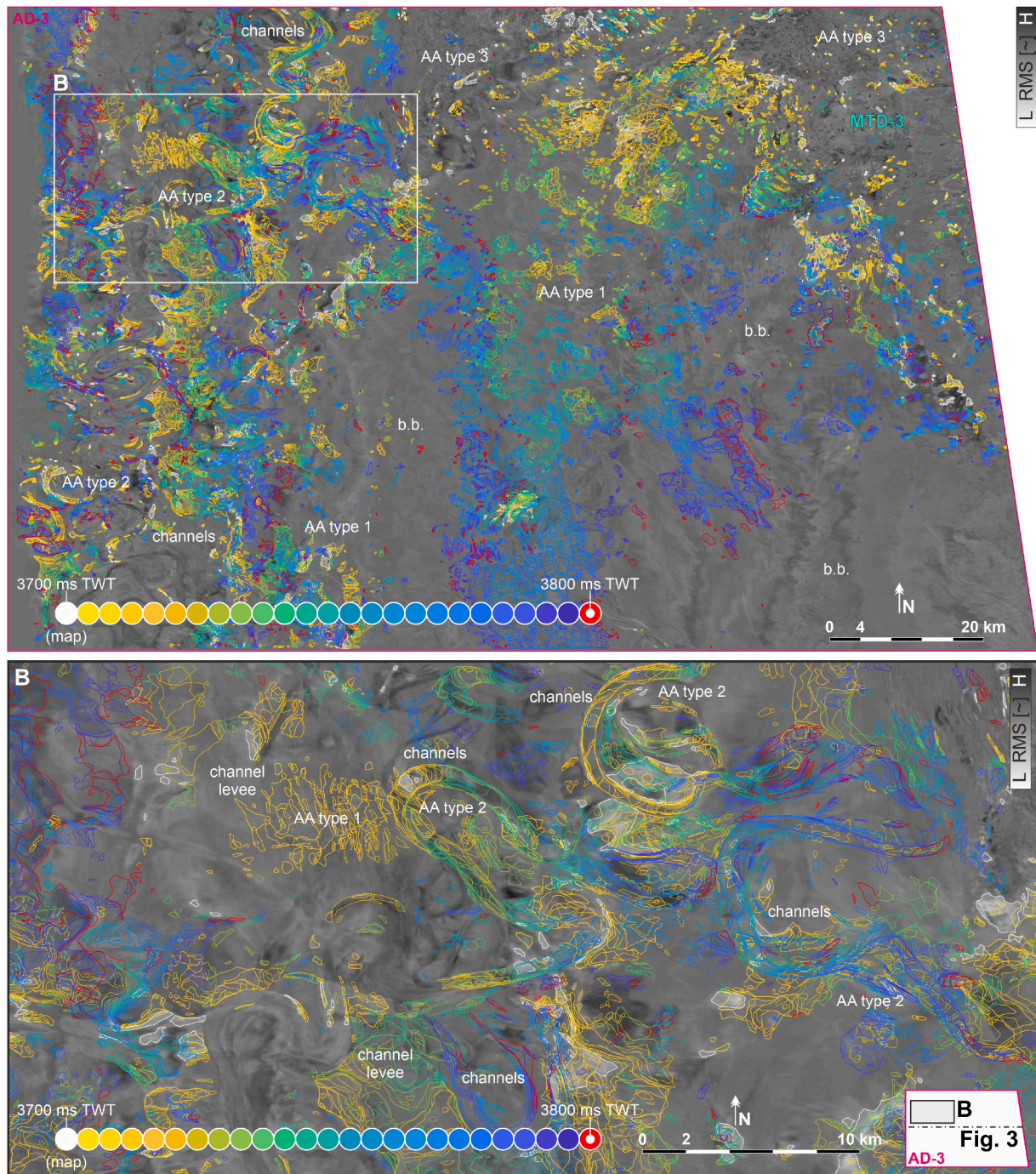

Fig. 5. Representative root-mean square (RMS) time slice at 3700 ms TWT (see Fig. 3A for map time-slice location), and close-up (B; see inset for close-up location), with superimposed the margins of the amplitude anomalies (AA) encountered within the interval between 3700 and 3800 ms TWT (spacing 4 ms TWT, 25 layers) (see Methods). The margins are color-coded with time (TWT). Staking of margins indicate either multiple anomalies or sliced anomalies. 3.4E4 anomalies have been encountered within this specific interval. Three main types of AA have been identified (see text). The anomalies do not fill the entire extent of the analyzed volume but are limited to small, charged proportions of channels (AA Type 2), channel levees (AA Type 1), and mass transport deposits (MTD) or background bedding (b.b.; AA Type 3).

4.2. Geophysical analysis of gas occurrences

4.2.1. Acoustic observations

More than seven hundred thousand (771,833) gas-related soft amplitude anomalies (AA) have been automatically detected from the 3-D seismic volume (see Methods). The AAs are characterized on seismic section by a high amplitude response with amplification well above the background one (Fig. 4, trace x). The AAs are here characterized by consecutive bright soft-hard pairs for each individual anomaly (Fig. 4A). The AAs exhibit a relative increase of the period of the wavelet and apparent downward bending near the centers of the amplitudes (push down, PD, Fig. 4). The diagnostic changes in wavelet and the downward bending are interpreted to be related to gas that reduces both, the higher frequency components of the seismic bandwidth (Castagna et al., 2003), and the compressional velocity of the seismic waves (Mavko et al., 2020), respectively.

The planform geometry of the individual AAs varies substantially in shape when observed on top view. For ease of description three types of AAs were defined and described with reference to representative examples shown in Fig. 5. The first type, called here AA type 1, shows a relatively rounded shape with irregular geometry and variable R (Fig. 5). The shape of these anomalies does not resemble any typical reservoir geobody and are hosted by the channel levees and by the more distal sediments derived from the paleo-Brahmaputra depositional system. AA type 2 are more elongated and characterized instead by a low R. These anomalies clearly conform to segments of meandering channels indicating gas-charge in the more porous and permeable proportions of channels (Fig. 5). AA type 3 are typically well rounded and characterized by higher R. These AAs are much smaller compared to the other two types and are associated with the sediments derived from the paleo-Brahmaputra deposits or found within the MTDs (Fig. 5).

Overall, the gas occurrences are laterally discontinuous. The representative subset of extracted AAs in Fig. 5 highlights that some proportion of the basin is indeed free from gas and that the eventual vertical migration of gas across the basin is expected to involve restricted proportions of the analyzed volume. These observations contrasts with many models presented in the literature where diffusion and advection of free phase methane is expected, and often modelled, as being laterally continuous and homogeneous for large portions of microbial basins (e. g., Kroeger et al., 2015). The three types of AAs are mostly organized in vertical ensembles composed by 2–3 to a few 10s of soft anomalies each (Figs. 3, 4 and 6). The AAs composing the vertical ensembles change shape from the base to the top of the anomaly stack. The anomalies are not evenly spaced and do not show even a systematic upward or downward size variation with depth (Figs. 3, 4 and 6). These characteristics point to a general "lack of rule" for the vertical succession of these stacked AAs.

Nevertheless, the stacked distribution of these soft anomalies resembles previously reported gas transport phenomena observed elsewhere, such as vertical anomaly clusters (VACs; Foschi et al., 2014, 2018) and pipes (Cartwright and Santamarina, 2015).

A laterally extensive soft anomaly located at a nearly constant distance of ~600 ms TWT (~550 m) from the seafloor surface (Figs. 3, 4 and 6) is observed over the central and the western portion of the study area. This soft anomaly cross cuts the background stratigraphy and is laterally continuous for several kilometers. Importantly, this laterally extensive anomaly represents the upper boundary of all the soft AAs observed in the study area. The acoustic characteristics of this bottom simulating reflection (BSR) are consistent with the response of the base of the gas hydrate stability zone (BGHSZ; Xu and Ruppel, 1999). The anomalies located immediately below this BSR are interpreted to indicate the presence of a free-gas zone (FGZ) (c.f. Bangs et al., 2003).

The BGHSZ was used to estimate the geothermal gradient in the study area. Previous estimates of the geothermal gradient in other locations of the Rakhine Basin were reported to be in the order of 29–30 °C/km (Barber et al., 2017; Basu et al., 2010). In the study area the BSR is located at ~560 m below seafloor (mbsf) and the BGHSZ, at this depth, is stable with a geothermal gradient of ~33 °C/km.
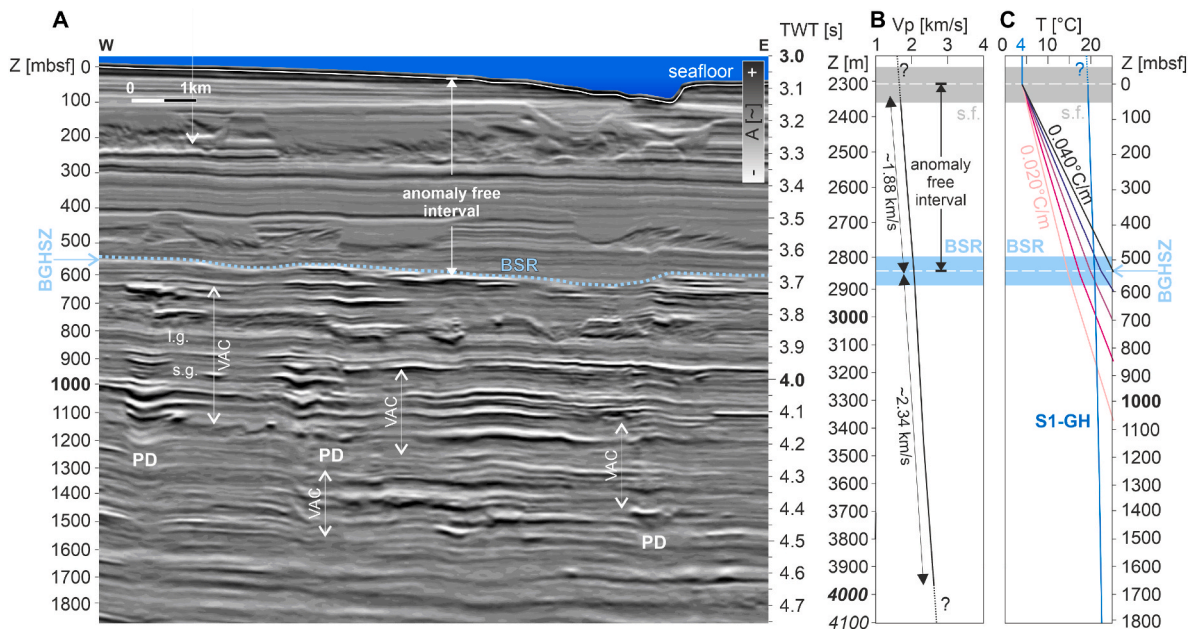

Fig. 6. (A) Seismic cross section (see Fig. 3 for line location) depicting stacked gas occurrences within the shallow section of the study area. The stacked gas occurrences, interpreted as vertical anomaly clusters (VACs) show variable sizes within the same ensemble and variable spacing between two consecutive occurrences in vertical succession (s.g. = short gap; l.g. = long gap). Most of the occurrences exhibit push-down (PD) associated with the presence of gas. A bottom simulating reflection (BSR) can be observed ~560 m below the seafloor. The BSR also represents a ceiling boundary for all encountered gas-related seismic anomalies. The BSR was interpreted as the base of the gas hydrate stability zone (BGHSZ). (B) The velocity profile was constructed using time-depth data provided by the operator (see Data and Method). The basin is characterized by velocities in the order of circa 1.9 to 2,3 km/s. (C) The depth of the bottom simulating reflection was used as proxy to calculate the geothermal gradient (see Materials and Methods). As observed in the modelling of Structure-I gas hydrate (S1-GH), a geothermal gradient of ~33 °C/km was obtained. The geothermal gradient curves from 25 to 40 °C/km are also shown for reference.

4.2.2. Vol, distribution, and roundness analysis

AV_{TS}, nAA_{TS}, and R (see Methods) were integrated to obtain an overall analysis of the gas distribution in the study area. AV_{TS} is clearly dominated by three intervals and has been used to describe the variation of the three parameters with depth. An additional interval, namely Interval 0, has been added to complete the description of the results from 3.25 to 3.50 s TWT. Interval 0 falls within the anomaly-free intervals and is associated with minor soft loops of hard anomalies related to the seafloor and other hard reflections. Interval 0 was excluded from the following descriptions and discussions.

Interval 1 extends from 3.50 to 3.65 s TWT. It is characterized by a sharp increase of AV_{TS} with a peak volume of 1.825 km^3 on a single time-slice. The sharp increase in AV_{TS} is also accompanied by an increase of nAA_{TS} to about 2870 units. R also increases over this interval from 0.17 to 2.1. Interval 1 occur mostly within the depth range of the BSR and the BGHSZ, from 3.50 to 3.75 s TWT. This interval also falls within the depth range of MTD-3 (from 3.25 to ~3.78 s TWT).

Interval 2 extends from 3.67 to 4.32 s TWT. The interval is characterized by a gradual decrease of AV_{TS} with depth, from its peak to about 0.3 km^3. Conversely, the upper part of the interval exhibits an increase of nAA_{TS} to its own peak of 3647 units at around 4 s TWT, followed by a gradual decrease to ~1750 units at base of Interval 2. R is relatively constant with values around 0.21 indicating similar type of geobodies characterized by comparable roundness. Interval 2 is characterized by two major local minima of both AV_{TS} and nAA_{TS}, at 3.90 and 4.10 s TWT. These minima are associated with the presence of MTD-2 and

MTD-1, respectively.

Interval 3 extends from 432 to 5.00 s TWT. This interval is characterized by small perturbations in AV_{TS}, with values ranging in the order of 0.2–0.5 km3 nAA_{TS} is characterized by a decrease of units (~500) up to 4.65 s TWT, and by a consecutive increase towards the bottom of the database where ~1650 units were detected. R increases from 4.32 to 4.70 s TWT and stabilizes at around 0.26 towards the base of the interval.

5. Discussion

5.1. Occurrence of microbial gas

The gas-related occurrences, as revealed by nAA_{TS}, are primarily distributed within Interval 2, which contains ~75% of all the encountered AAs within the study area. The volume of the gas related amplitude anomalies stored in Interval 2, as shown by AV_{TS}, is more than twice the volume calculated within the underlying Interval 3. These results suggest the presence of a supercharged section of the basin that coincides with the defined Interval 2, from below the BGHSZ to ~4325 ms TWT (Fig. 7), or from ~560 to 1300 mbsf (Fig. 8). Conversely, Interval 3 hosts about 20% of the anomalies and could indicate a region of past microbial generation (now buried) or a depleted region from where all gas moved away (discussed later).

Interval 2, using the geothermal gradient of 0.033 °C/m derived from the BGHSZ (Fig. 6), is characterized by a temperature interval of ~22 °C
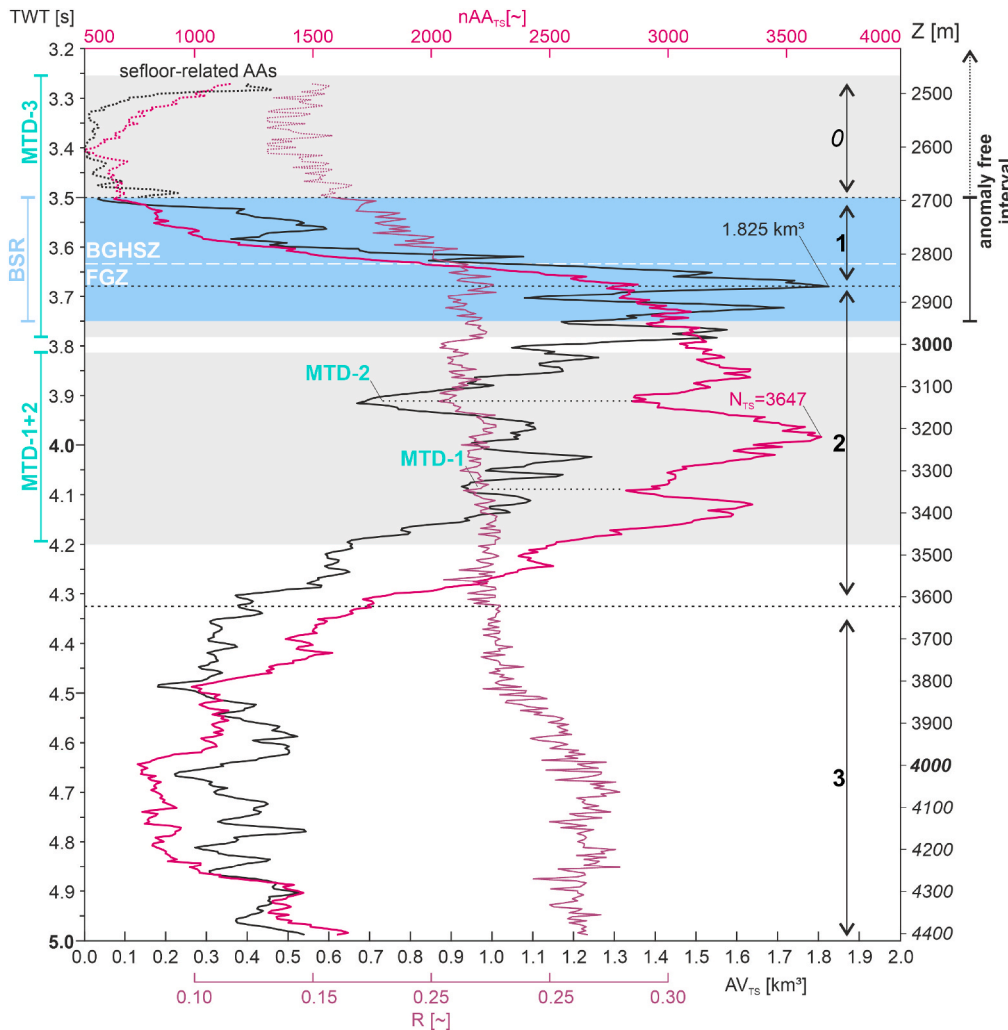

Fig. 7. Cross plot with cumulative amplitude volume of the gas-related amplitude anomalies per time-slice, AV_{TS}, number of amplitude anomalies (AA) per time-slice, nAA_{TS}, and roundness of the anomalies, R (see Methods), with depth range of mass transport deposits (MTD) and bottom simulating reflection (BSR). Three main intervals (1–3, black arrows) define the overall distribution and characteristics of the gas occurrences found in the study area (see text). The BSR separates the base of the gas hydrate stability zone (BGHSZ) and the free-gas zone (FGZ).
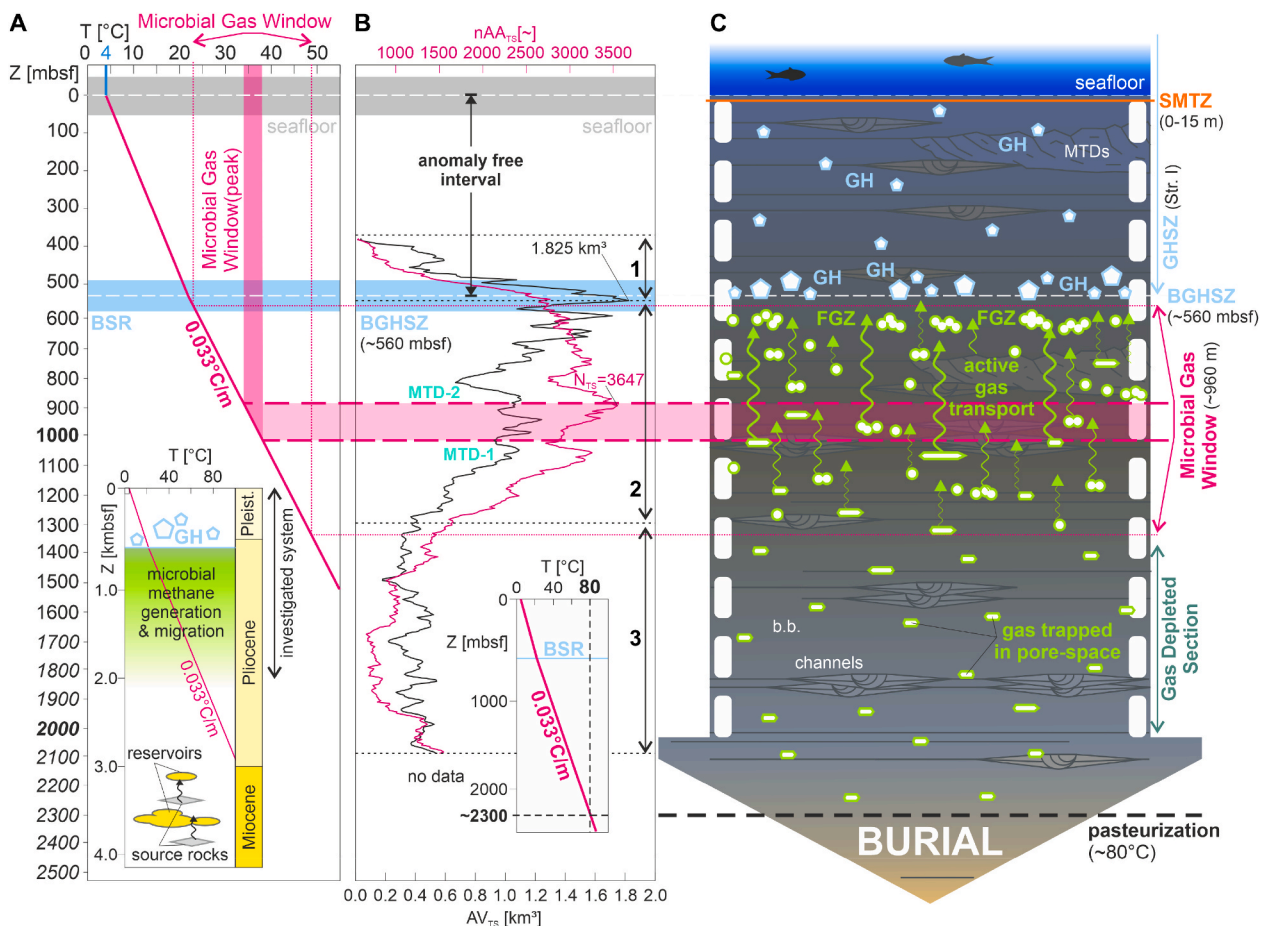
Fig. 8. (A) Temperature-depth (T–D) plot shows the average depths of seafloor and bottom simulating reflection (BSR). The microbial generation window (MGW) is consistent with a temperature range of 23–49 °C with a peak methane generation around 34–38 °C (see text). The investigated system is part of a broader petroleum system that includes deeper Miocene source rocks (S.R.) and sand-rich reservoirs (res.) (see text). (B) Using a geothermal gradient of 0.033 °C/m (from BSR, see Fig. 6) a depth range of 571–1336 m below seafloor (mbsf) is obtained. The peak of microbial gas generation is expected at a depth of 947 mbsf. The pasteurization temperature of 80 °C is located at around 2300 mbsf (inset). The gas occurrences indicators and the interpreted intervals are compared with the resulting MGW, and the average depths of mass transport deposits (MTD). Interval 2 fits with the depth of gas generation (MGW). The seals acting in the basin are the MTDs which restrict only partially the fluid transport towards the gas hydrate stability zone (GHSZ) (AV_{TS} = gas-related anomaly volume per time-slice; , nAA_{TS} = number of amplitude anomalies per time-slice). (C) Synoptic diagram of the microbial gas system in the Rakhine Basin showing a sedimentary column undergoing burial. The depths of the sulphate methane transition zone (SMTZ), the base of the GHSZ (BGHSZ) and the depth of the MGW are fixed in time and at fixed distance with respect to the seafloor. Gas generation in the MGW is followed by transport towards the BGHSZ producing stacked gas occurrences (green circles and arrows). The trapped gas occurrences (green squares and rectangles) are subject to burial with the rest of the sedimentary column. The upward gas transport produces the lower gas depleted section (GDS). Large gas hydrate (GH) occurrences (pentagons) are present near the BGHSZ and are sourced from allochthonous gas derived from the MGW; minor GH pockets precipitate within the GHSZ. The synoptic diagram does not include horizontal migration and diffusion of microbial gas. The background drawings of channels, background bedding (b.b.), and MTDs is qualitative.

and ~47 °C, from top to base, respectively (Fig. 8). This fits the temperature range derived from modelling of microbial methanogenesis in the Rakhine Basin, which occurs between 23 and 49 °C (Chung et al., 2012), and importantly it fits with previously reported microbial temperature windows, characterized by peak of methane generation around 34–38 °C (e.g., Schulz and Conrad, 1996; Schulz et al., 1997; Yao and Conrad, 2000; Katz, 2011). It is worth nothing that the reconstructed temperature of peak gas generation in the study area (34–38 °C at a depth of 900–1000 mbsf) nearly matches the depth of the documented peak in nAA_{TS} (~900 mbsf, Fig. 8).

AV_{TS} shows that the largest volume of gas-related anomalies is located at the top of Interval 2 with peak just below the BGHSZ (Fig. 8). The peak in AV_{TS} is ~340 m above the expected peak of gas generation previously mentioned indicating that some form of transport is active in the study area. Indeed, it is conceivable that if (i)a mechanism of transport was not present in the basin and (ii)that methanogenesis was followed by an in-situ charge of gas into the source layers, the two peaks in nAA_{TS} and AV_{TS} would have been located at similar depths. The

upward gradual increase in AV_{TS} in Interval 2 rules out this unlikely scenario and argue positively for a vertical gas transport active in the basin.

It is worth noting that the roundness R is nearly constant in Interval 2 (Fig. 7), indicating that the gas occurrences are hosted by an equal proportion of channels, channel-levees and background strata with depth. Again, a variable proportion of these host formations and geobodies with depth would have been expressed as a more variable R along Interval 2.

5.2. Combining geophysical and geochemical data to confirm the gas origin

The gas system of the Rakhine Basin was considered microbial because of the molecular and isotopic composition of the gas from Pliocene reservoirs (99% CH_4, $\delta^{13}C$–CH_4 from −59 to −70‰; see Section 2) and the immature character of the Pliocene sediments, with vitrinite reflectance values ranging from 0.1% at 1000 m, to 0.4% at ~3200 m.

The isotopic data of Chung et al. (2012) have been plotted on the updated isotopic genetic diagram of Milkov and Etiope (2018), which clearly confirms a dominant microbial origin related to carbonate reduction (CR; Fig. 9). The diagram, however, also shows that methane becomes enriched with depth, reaching CH_4 values of -42‰. The distribution of the isotopic data suggests a minor mixing trend with thermogenic gas, likely attributable to the Miocene source rocks. We cannot exclude therefore that a minor component of this thermogenic gas migrates (and therefore it is allochthonous in the studied portion of the basin), mixes with the dominant microbial gas and reaches the surface. Although also early mature thermogenic gas can be ^{13}C-depleted, resembling microbial gas (Milkov and Etiope, 2018), the isotopic and compositional data of Rakhine gas exclude this possibility; this is consistent with the very low maturity indexes and temperatures reported above.

Our geophysical data reach a depth of about 2100 m, approaching approximately the middle Pliocene formations, as suggested by the nearest well log (Rubis-1 well) reported in Racey and Ridd (2015). This depth would correspond to a present temperature of 56 °C, using the average geothermal gradient of the Rakhine Basin (25 °C/km; Racey and Reed, 2015). The thermal gradient derived above using the BSR of the GHSZ in the seismic data (33 °C/km, Fig. 6) would suggest, for the depth of 2100 m, a temperature of 73 °C. This is similar with the temperature of 60 °C at a depth of 2000 m, derived by the modelling of Chung et al. (2012). Assuming that the acoustic anomalies not related to VACs refer to gas generated in situ, as discussed in Section 5.1, the low levels of temperature and vitrinite derivable maturity (0.1–0.3%) would clearly indicate generation of microbial gas, practically only methane. It is plausible to assume that the isotopic composition of this methane is not more ^{13}C-enriched than the lowest $\delta^{13}C–CH_4$ value measured in the deeper Pliocene sandstone reservoirs (-70‰). This gas then migrates upwards and towards the shallow section of the basin.

5.3. Evidence of gas transport

The presence of VACs and other stacked anomalies are typically associated with sequential vertical gas migration across multi-layered sequences (c.f. Foschi et al., 2014) and have been observed in both
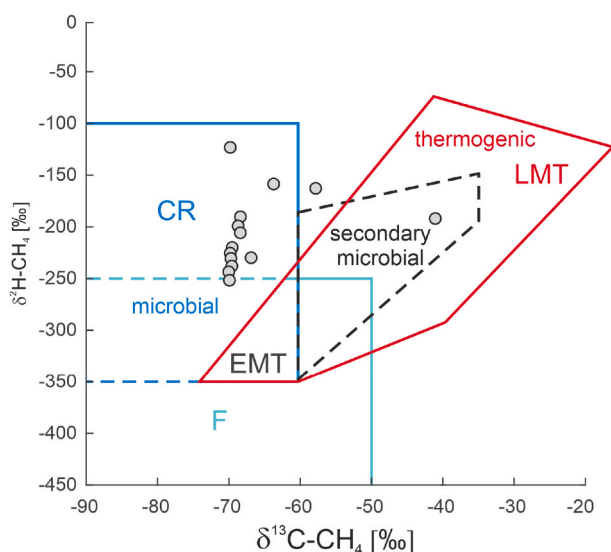

Fig. 9. Stable carbon and hydrogen isotope ratios of methane in the Rakhine Basin (data from Chung et al., 2012) in the framework of genetic fields proposed by Milkov and Etiope (2018). The result shows that the origin of the gas is microbial and related to carbonate reduction (CR) methanogenesis. EMT = early mature thermogenic; LMT = late mature thermogenic; F = methyl-type fermentation.

coarse heterolothic formations (Foschi et al., 2018) and seal and caprock-related lithologies (Bertoni et al., 2018; Foschi and Van Rensbergen, 2022). We do not exclude that other forms of gas transport, such as pipes (Cartwright and Santamarina, 2015) might be present in the basin. The presence of VACs and stacked anomalies within the Pliocene-Pleistocene shale formations are postulated to be representative of the microbial gas production, in-situ within Interval 2, but also indicative of gas transport across strata.

The presence of MTDs has been observed to reduce both the distribution (nAA_{TS}) and the volume of the gas occurrences (AV_{TS}) (Fig. 8). The two local minima located at a depth of 850 and 1000 mbsf (Fig. 8; at 3.90 and 4.10 s TWT in Fig. 7) could indicate that gas coming from below the MTD could be temporarily, or partially, trapped by the reworked facies that characterize these kind of deposits. This hypothesis finds confirmation by the observed increase-to-sharp-decrease trend of the distribution and volume of the anomalies across the base of the MTDs (Fig. 7). Nevertheless, it is worth nothing that the overall trends within Interval 2 are maintained, suggesting a limited sealing potential of the two MTDs.

Considering the entire sequence as capable of sustaining long-range and long-term advection of free-phase methane, it is conceivable that all gas charged into Interval 2 must balance with a depleted section located underneath (Fig. 8). Interval 3, as previously anticipated in section 5.1, could well represent a region of residual gas where small occurrence of gas remain trapped and subject to burial. Although this argument remains speculative, the presence of a gas-depleted section could well be expressed by the limited variation of both in nAA_{TS} and AV_{TS} in this specific interval (gas-depleted section, Fig. 8).

Due to the lack of clear images of faults or fracture systems, we hypothesize that the gas may migrate by a combination of capillary invasion (Jain and Juanes, 2009) and gas-phase advection along fractures that are not seismically resolvable. Vertically aligned acoustic anomalies can, in fact, be interpreted as acoustic pipes representing fracture pathways (Cartwright and Santamarina, 2015). Notwithstanding claystones are generally considered to have low permeability, gas advection has been documented in clayey rocks, especially in the framework of the studies on clays as barriers in nuclear waste repositories (e.g., Volckaert et al., 1993; Horseman et al., 1999; Etiope and Martinelli, 2002; Graham et al., 2002). Systems of micro-fractures and fissures can, in fact, develop within solidified clay sediments due to gas pressure build-up (e.g., Tamayo-Mas et al., 2021). These fisssures can be "invisible" to seismic data depending on the anisotropy of the rock and the rheology and orientation of the fractures (e.g., Grechka and Tsvankin, 2003). Such an evidence of massive gas migration towards the surface leaves little room for the alternative hypothesis that hydrates host gas produced by in-situ methanogenesis, as frequently reported in other areas (e.g., Malinverno, 2010).

5.4. Gas trapping in surface hydrates

The peak in AV_{TS} observed below the BGHSZ followed by the onset of the anomaly-free interval observed on seismic data (Figs. 4 and 6) strongly suggests that the formation of gas hydrates is such that the microbial gas cannot migrate further to either precipitate inside the GHSZ or move fast across the GHSZ and reach the seafloor (Liu and Flemings, 2007). There is no substantial evidence of hard reflections in the upper portion of Intervals 1 and 0 that could justify the interpretation of gas hydrate deposits. The latter are then expected to form only immediately above the FGZ and within the lower portion of Interval 1 (Figs. 4 and 6). The gas hydrates in the Rakhine Basin are, then, here regarded as the ultimate seal for the entire petroleum system. It cannot be excluded, however, that minor fractions of hydrates within the GHSZ may host *in-situ* produced methane (autochthonous).

6. Conclusions

High-resolution 3-D seismic data allowed to investigate a gas-charged sedimentary system of the Rakhine Basin, spanning from surface gas hydrate accumulations to a depth of about 2 km. This system is part of a wider, and deeper, Miocene to Pliocene petroleum system. Specifically, the geophysical data allowed to discover that the gas hosted in the shallow gas hydrates migrated from deeper supercharged sediments, hosting hundreds of thousands of occurrences of gas of microbial origin, as indicated by geochemical data and the present-day optimum temperature for microbial methanogenesis. Active free-phase gas migration from gas-charged formations towards the shallow GHSZ, is imaged on seismic data as stacked amplitude anomalies and vertical anomaly clusters, although the investigated portion of the basin does not host fluid reservoirs, and evident fault systems, which are instead observed on other studies (e.g., Yang et al., 2021). The GHSZ acts as the ultimate seal for the entire petroleum system.

The gas hydrates in the Rakhine Basin represent a peculiar case of structural hydrate deposit with microbial allochthonous gas and can be considered as a case of "frozen seepage" of microbial gas with relatively high flux and pressure. Without the integrated approach used in this work, combining gas geochemical and geophysical data of the entire regional gas-bearing sedimentary system, the shallow gas hydrates of the Rakhine Basin could have been misinterpreted as *in-situ* produced microbial gas occurrences.

Declaration of competing interest

The authors declare that they have no known competing financial interests or personal relationships that could have appeared to influence the work reported in this paper.

Data availability

The data that has been used is confidential.

Appendix A. Supplementary data

Supplementary data to this article can be found online at https://doi.org/10.1016/j.marpetgeo.2023.106100.

References

Adhikari, S.K., Sakai, T., Yoshida, K., 2018. Data report: grain size analysis of Bengal Fan sediments at Sites U1450 and U1451, IODP Expedition 354. Proceedings of the International Ocean Discovery Program 354.

BP, 2021. Statistical review of world energy. https://www.bp.com/en/global/corporate/energy-economics/statistical-review-of-world-energy.html, 70th edition.

Bangs, N.L., Sawyer, D.S., Golovchenko, X., 1993. Free gas at the base of the gas hydrate zone in the vicinity of the Chile triple junction. Geology 21 (10), 905–908.

Barber, A.J., Zaw, K., Crow, M.J., 2017. The pre-Cenozoic tectonic evolution of Myanmar. Geological Society 48 (1), 687–712. London, Memoirs.

Basu, P., Verma, R., Paul, R., Viswanath, S., 2010. February. Deep waters of Rakhine Basin. A new frontier. In: 8th Biennial International Conference and Exposition on Petroleum Geophysics, p. P160. Hyderabad.

Beauchamp, B., 2004. Natural gas hydrates: myths, facts and issues. Compt. Rendus Geosci. 336, 751–765.

Bertoni, C., Cartwright, J., Foschi, M., Martin, J., 2018. Spectrum of gas migration phenomena across multilayered sealing sequences. AAPG (Am. Assoc. Pet. Geol.) Bull. 102 (6), 1011–1034.

Brown, A.R., 2011. AAPG Memoir 42 SEG Investigations in Geophysics, No. 9. In: Interpretation of Three-Dimensional Seismic Data. The American Association of Petroleum Geologists and the Society of Exploration Geophysicists, Tulsa, Oklahoma, U.S.A.

Brown Jr., L.F., Fisher, W.L., 1977. Seismic-stratigraphic Interpretation of Depositional Systems: Examples from Brazilian Rift and Pull-Apart Basins: Section 2. Application of Seismic Reflection Configuration to Stratigraphic Interpretation.

Cartwright, J., Santamarina, C., 2015. Seismic characteristics of fluid escape pipes in sedimentary basins: implications for pipe genesis. Mar. Petrol. Geol. 65, 126–140.

Castagna, J.P., Sun, S., Siegfried, R.W., 2003. Instantaneous spectral analysis: detection of low-frequency shadows associated with hydrocarbons. Lead. Edge 22 (2), 120–127.

Chung, Y.H., Yang, S.Y., Kim, J.W., 2012. Numerical simulation of deep biogenic gas play northeastern Bay of Bengal, offshore northwest Myanmar. In: AAPG International Conference and Exhibition (Milan).

Cliff, D., Carter, P., 2016. Exploration of the Rakhine Basin, Pushing Out the Barriers with New 3D: AAPG Search and Discovery Article 10848.

Dillon, W.P., Nealon, J.W., Taylor, M.H., Lee, M.W., Drury, R.M., Anton, C.H., 2001. Seafloor collapse and methane venting associated with gas hydrate on the Blake Ridge – causes and implications to seafloor stability and methane release. In: Paull, C.K., Dillon, W.P. (Eds.), Natural Gas Hydrates: Occurrence, Distribution, and Detection. American Geophysical Union, Washington, DC, pp. 211–233.

Etiope, G., 2015. Natural Gas Seepage. The Earth's Hydrocarbon Degassing. Springer, Switzerland.

Etiope, G., Martinelli, G., 2002. Migration of carrier and trace gases in the geosphere: an overview. Phys. Earth Planet. In. 129 (3–4), 185–204.

Foschi, M., Van Rensbergen, P., 2022. Topseal integrity assessment using seal properties and leakage phenomena. Mar. Petrol. Geol. 139, 105573.

Foschi, M., Cartwright, J.A., Peel, F.J., 2014. Vertical anomaly clusters: evidence for vertical gas migration across multilayered sealing sequences. AAPG (Am. Assoc. Pet. Geol.) Bull. 98 (9), 1859–1884.

Foschi, M., Cartwright, J.A., MacMinn, C.W., 2018. Sequential vertical gas charge into multilayered sequences controlled by central conduits. AAPG (Am. Assoc. Pet. Geol.) Bull. 102 (5), 855–883.

Graham, J., Halayko, K.G., Hume, H., Kirkham, T., Gray, M., Oscarson, D., 2002. A capillarity-advective model for gas break-through in clays. Eng. Geol. 64, 273–286.

Grechka, V., Tsvankin, I., 2003. Feasibility of seismic characterization of multiple fracture sets. Geophysics 68 (4), 1399–1407.

Hongxia, M., Fuliang, L., Guozhang, F., Hui, S., Cuixin, G., 2011. Seismic responses and geological characteristics of mass transport deposits in the Rakhine Basin, offshore Myanmar. Oil Gas Geol. 32, 751–759 (In Chinese with English summary).

Horseman, S.T., Harrington, J.F., Sellin, P., 1999. Gas migration in clay barriers. Eng. Geol. 54, 139–143.

Jain, A.K., Juanes, R., 2009. Preferential mode of gas invasion in sediments: grain-scale mechanistic model of coupled multiphase fluid flow and sediment mechanics. J. Geophys. Res. Solid Earth 114 (B8).

Katz, B.J., 2011. Microbial processes and natural gas accumulations. Open Geol. J. 5 (1).

Kroeger, K.F., Plaza-Faverola, A., Barnes, P.M., Pecher, I.A., 2015. Thermal evolution of the New Zealand Hikurangi subduction margin: impact on natural gas generation and methane hydrate formation–A model study. Mar. Petrol. Geol. 63, 97-114.

Kvenvolden, K.A., 1995. A review of the geochemistry of methane in natural gas hydrate. Org. Geochem. 23 (11–12), 997–1008.

Liu, X., Flemings, P.B., 2007. Dynamic multiphase flow model of hydrate formation in marine sediments. J. Geophys. Res. Solid Earth 112 (B3).

Malinverno, A., 2010. Marine gas hydrates in thin sand layers that soak up microbial methane. Earth Planet Sci. Lett. 292 (3–4), 399–408.

Mavko, G., Mukerji, T., Dvorkin, J., 2020. The Rock Physics Handbook. Cambridge university press.

Milkov, A.V., 2005. Molecular and stable isotope compositions of natural gas hydrates: a revised global dataset and basic interpretations in the context of geological settings. Org. Geochem. 36, 681–702.

Milkov, A.V., Etiope, G., 2018. Revised genetic diagrams for natural gases based on a global dataset of> 20,000 samples. Org. Geochem. 125, 109–120.

Monteleone, V., Marín-Moreno, H., Bayrakci, G., Best, A., Shaon, F., Hossain, M.M., Al Karim, A., Alam, M.K., 2022. Seismic characterization and modelling of the gas hydrate system in the northern Bay of Bengal, offshore Bangladesh. Mar. Petrol. Geol. 141, 105690.

Nielsen, C., Chamot-Rooke, N., Rangin, C., 2004. From partial to full strain partitioning along the Indo-Burmese hyper-oblique subduction. Mar. Geol. 209 (1–4), 303–327.

Paull, C.K., Brewer, P.G., Ussler III, W., Peltzer, E.T., Rehder, G., Clague, D., 2003. An experiment demonstrating that marine slumping is a mechanism to transfer methane from seafloor gas-hydrate deposits into the upper ocean and atmosphere. Geo Mar. Lett. 22, 198–203.

Racey, A., Ridd, M.F., 2015. Petroleum geology of the Rakhine region, Myanmar. Geological Society 45 (1), 93–108. London, Memoirs.

Ruppel, C.D., Kessler, J.D., 2017. The interaction of climate change and methane hydrates. Rev. Geophys. 55, 126–168. https://doi.org/10.1002/2016rg000534.

Schneider, F., Dubille, M., Montadert, L., 2016. Modeling of microbial gas generation: application to the eastern Mediterranean" Biogenic Play. Geol. Acta 14 (4), 0403-417.

Schulz, S., Conrad, R., 1996. Influence of temperature on pathways to methane production in the permanently cold profundal sediment of Lake Constance. FEMS Microbiol. Ecol. 20, 1–14.

Schulz, S., Matsuyama, H., Conrad, R., 1997. Temperature dependence of methane production from different precursors in a profundal sediment (Lake Constance). FEMS Microbiol. Ecol. 22, 207–213.

Skene, K.I., Piper, D.J., Hill, P.S., 2002. Quantitative analysis of variations in depositional sequence thickness from submarine channel levees. Sedimentology 49 (6), 1411–1430.

Sloan Jr., E.D., Koh, C.A., 2007. Clathrate Hydrates of Natural Gases. CRC press.

Tamayo-Mas, E., Harrington, J.F., Brüning, T., Shao, H., Dagher, E.E., Lee, J., et al., 2021. Modelling advective gas flow in compact bentonite: lessons learnt from different numerical approaches. Int. J. Rock Mech. Min. Sci. 139, 104580.

Volckaert, G., Put, M., Ortiz, L., De Canniere, P., Horseman, S.T., Harrington, J., Fioravante, V., Impey, M., Worgan, K., 1993. Megas, Modelling and experiments on gas migration in repository host rocks. In: Proceedings of the Meeting of Koln on PEGASUS Project. CEC EUR Series, 3–4 June 1993.

Whiticar, M.J., 2020. The biogeochemical methane cycle. In: Wilkes, H. (Ed.), Hydrocarbons, Oils and Lipids: Diversity, Origin, Chemistry and Fate, Handbook of Hydrocarbon and Lipid Microbiology. Springer Nature Switzerland AG, pp. 669–746. https://doi.org/10.1007/978-3-319-90569-3_5.

Widess, M.B., 1973. How thin is a thin bed? Geophysics 38 (6), 1176–1180.

Xu, W., Ruppel, C., 1999. Predicting the occurrence, distribution, and evolution of methane gas hydrate in porous marine sediments. J. Geophys. Res. Solid Earth 104 (B3), 5081–5095.

Yamamoto, A., Yamanaka, Y., Tajika, E., 2009. Modeling of methane bubbles released from large sea-floor area: condition required for methane emission to the atmosphere. Earth Planet Sci. Lett. 284, 590–598.

Yamamoto, K., Wang, X.X., Tamaki, M., Suzuki, K., 2019. The second offshore production of methane hydrate in the Nankai Trough and gas production behavior from a heterogeneous methane hydrate reservoir. RSC Adv. 9 (45), 25987–26013.

Yamano, M., Uyeda, S., Aoki, Y., Shipley, T.H., 1982. Estimates of heat flow derived from gas hydrates. Geology 10 (7), 339–343.

Yang, J., Lu, M., Yao, Z., Wang, M., Lu, S., Qi, N., Xia, Y., 2021. A Geophysical Review of the Seabed Methane Seepage Features and Their Relationship with Gas Hydrate Systems. Geofluids, 2021.

Yao, H., Conrad, R., 2000. Effect of temperature on reduction of iron and production of carbon dioxide and methane in anoxic wetland rice soils. Biol. Fertil. Soils 32 (2), 135-141.

You, K., Flemings, P.B., Malinverno, A., Collett, T.S., Darnell, K., 2019. Mechanisms of methane hydrate formation in geological systems. Reviews of Geophysics 57 (4), 1146–1196.